All-fiber phase modulator and switch based on LSPR effect of the AuNPs embedded in Gel membrane

Meng Luo[a], Xinghua Yang[a,*], Pingping Teng[a], Zhihai Liu[a], Jun Yang[a], Depeng Kong[b], Danheng Gao [a], Zhanao Li[a], Xingyue Wen[a], Ximiao Yu[a],Libo Yuan[a,c], Kang Li[d], Mark Bowkett[d], NigelCopner[d], Xiaozhang Wang[e]

[a]*Key Lab of In-Fiber Integrated Optics, College of Science, Harbin Engineering University, Harbin 150001, China*
[b]*State Key Lab of Transient Optics and Photonics, Xi'an Institute of Optics and Precision Mechanic, Chinese Academy of Sciences, Xi'an 710119, China*
[c]*Photonics Research Center, Guilin University of Electronics Technology, Guilin 541004, China*
[d]*Wireless & Optoelectronics Research & Innovation Centre, Faculty of Computing, Engineering & Science, University of South Wales, Wales, CF37 1DL, UK*
[e]*Xi'an Modern Control Technology Research Institute, Xi'an, 710065, China*
**Corresponding author: yangxh@hrbeu.edu.cn*

Received Month X, XXXX; revised Month X, XXXX; accepted Month X, XXXX; posted Month X, XXXX (Doc. ID XXXXX); published Month X, XXXX

All-fiber modulators and switches have drawn great interest in photonics domain, and they are applied in viable photonic and optoelectronic devices. In this work, with the assistance of agarose membrane, aspherical gold nanoparticles are embedded on the surface of the microfiber treated with the piranha solution. An all-fiber Mach-Zehnder interferometer was used to realize a low-cost, low-loss, and conveniently prepared all-fiber phase modulator. By taking advantage of local surface plasmon resonance effect of gold nanoparticles embedded in agarose membrane, under the excitation of near-infrared region light, the gold nanoparticles were excited to change the effective refractive index of one arm of the Mach-Zehnder interferometer. A maximum phase shift of ~6π at 1550 nm was obtained from the device. Besides, an all-optical switch was achieved with rising edge time of 47 ms and falling edge time 14 ms. The proposed all-fiber modulator and switch based on the local surface plasmon resonance effect of gold nanoparticles embedded in agarose membrane will provide great potentials in all-optical fiber system. © 2020 Optical Society of America

OCIS Codes: 000.0000, 999.9999

1. Introduction

All-optical devices have drawn more and more attention with its high speed and low loss [1, 2]. With the unremitting efforts of researchers, many all-optical devices have been fabricated and applied in many fields, such as all-optical routing [3,4], modulator [5,6] , and optical logic gate [7-10]. All-fiber devices play a key role in all-optical devices [11,12], because they are more suitable for integrating fiber lasers, wavelength-division multiplexing (WDM) fiber communication systems, and fiber-sensing systems. Among them, all-fiber phase modulators have drawn increasingly interesting due to their unique function. Upon to now, all-fiber modulators based on different mechanisms, such as electro-optic effect [13-16], thermo-optic effect [17,18], and photo-thermal effect, have been designed. A commendable effort to realize all-fiber modulator based on graphene has been proposed [19], but it suffers from high loss. Therefore, a low-loss all-fiber modulator is urgently needed.

In the past few decades, with the witness advance significant progress of nanoscience, various nanoscale photo-thermal conversion materials have been reported and pursued in many fields such as photo-thermal therapy, image, and SERS (surface enhanced Raman spectroscopy) detect [20-22]. Due to the unique local surface plasmon resonance (LSPR) characteristics, plasmonic nanoparticles have attracted more attention of researches. Especially, gold nanoparticles (AuNPs) with their excellent physical and chemical properties have been applied in many fields, such as drug delivery [23], cancer treatment [24], and sensing [25]. By varying the size and geometry, AuNPs show different photonic properties, for example, spectral absorption which is very important for realizing a low-loss all-fiber phase modulator.

In this paper, an all-fiber phase modulator based on LSPR absorption of AuNPs was demonstrated. The device was fabricated by depositing AuNPs embedded in the agarose membrane on the microfiber arm of a Mach-Zehnder interferometer (MZI). The free electrons in the plasmon band of AuNPs were excited by the near-infrared region (NIR) light through the evanescent field of the microfiber stereo structure, then excited electrons relaxed to the ground state and release heat. Finally, the temperature of the waist region of microfiber was increased resulting in a change in the effective refractive index (RI). Parallel to this, the changes of the phase difference of the MZI caused interference spectrum phase shifts. Meanwhile, the proposed all-fiber modulator can be applied as an all-optical switch, which has intrinsic compatibility with the current all-fiber system [26]. Hence, the proposed all-fiber device with low loss and low cost has good application potential for all-optical communication.

2. Experiment

The AuNPs were provided by Nanjing Jike Biotechnology Co., Ltd.. It was a stable aqueous suspension with rose-like color. The AuNPs present a rod structure as shown in the transmission electron microscope (TEM) image of Fig. 1 (a). The transverse size of the AuNPs is ~20 nm and the longitudinal size is ~80 nm, respectively. The absorption

spectrum of AuNPs is shown in Fig. 1 (b). The absorption peak is ~794 nm and the half-value width is ~168 nm. The inset shows that in the NIR spectral range, the numerical simulation result of the transverse absorption mode of AuNPs shows that the electric field intensity around the cross-section of AuNPs is significantly enhanced. The result indicates that AuNPs have strong LSPR absorption. Agarose is a polymer that is widely present in algae and has been widely used in the field of biochemistry [27], electro-chemical [28], and sensor [29]. Agarose contains large numbers of hydroxyl groups. What's more, the agarose membrane has good optical permeability. The microfiber prepared by the autonomous tapering machine was treated with piranha solution to expose the surface hydroxyl groups. Under the combination of hydrogen bonds, the agarose gel can be uniformly and firmly coated on the surface of the microfiber. In this experiment, AuNPs were embedded in the agarose membrane. Through this convenient method, AuNPs can be firmly fixed on the surface of microfiber. The preparing processes are as follows: 0.25 g agarose powder (Biowest Agarose) was mixed into 100 ml deionized water and heated to 90 °C to form a homogeneous solution. 1 ml AuNPs solution was centrifuged at 3000 rpm for 3 minutes to remove the supernatant, then the AuNPs obtained by centrifugation were added to the 0.5 ml prepared agarose solution at about ~45 °C and sonicated to a uniform. A droplet of AuNPs agarose solution slowly spread along the tapered region of microfiber using a syringe and leave to dry for 24 h. The microscopic image is shown in the dotted frame of the Fig. 2.

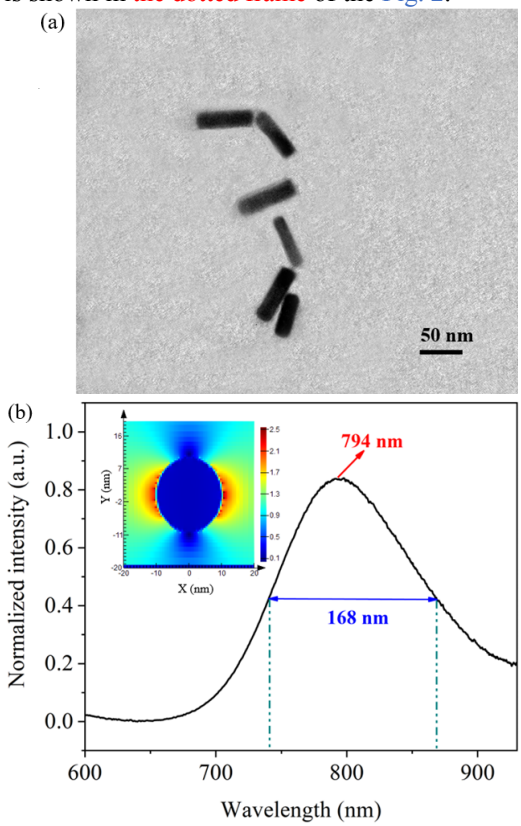

Fig. 1 (a) NIR absorption spectrum of AuNPs, the inset is the result of simulation of the AuNPs. (The white dotted frame represents AuNPs). (b) TEM image of AuNPs.

The experimental device schematic diagram is shown in Fig. 2. The MZI was composed of two 1×2 3 dB optical couplers (50/50) and a variable optical attenuator (VOA). The prepared microfiber coated with AuNPs embedded in the agarose membrane was deposited on one arm of the MZI. A broadband signal light emitted by an amplified spontaneous emission (ASE) with a range of 1520 nm to 1610 nm was guided into the MZI, and a laser with a center wavelength of 808 nm was injected into the arm of MZI with the microfiber through a WDM coupler. By adjusting the knob of VOA, a comb spectrum with a greater interference contrast was obtained as shown in the black curve of Fig. 3. The free spectral range (FSR) of the interference spectrum is ~0.89 nm. The output intensity of the MZI is calculated from as follow [30]:

$$I = I_1 + I_2 + 2\sqrt{I_1 I_2}\cos(\Delta\varphi) \quad (1)$$

$$\Delta\varphi = \frac{2\pi}{\lambda}\Delta nL \quad (2)$$

I_1 and I_2 present the intensity of the two arms which were divided by the optical coupler. The optical wavelength is present by λ. L is the different length of the two arms of MZI, and Δφ is the phase difference which can be controlled by the Δn, which represents the effective RI difference of two arms of the MZI.

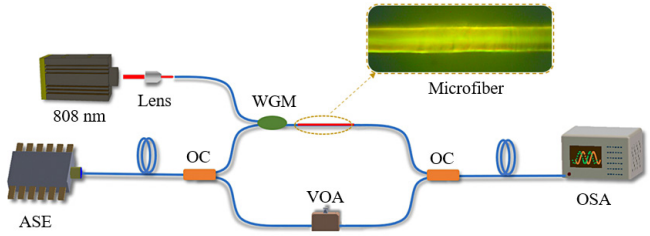

Fig. 2 The setup of proposed all-fiber phase modulator; ASE: amplified spontaneous emission; WDM: wavelength-division multiplexing; OC; optical coupler; VOA: variable optical attenuator; OSA: optical spectrum analyzer.

3. Experimental results and discussion

When the 808 nm laser was guided into the MZI, the free electrons in the plasmon band of AuNPs were excited by the NIR light through the evanescent field of the microfiber structure, then the effective RI of the waist region of microfiber was changed by the thermo-optic effect resulting in the optical path difference of MZI to change. Therefore, the phase of the interference spectrum recorded by the optical spectrum analyzer (OSA) was shifted. As the power of 808 nm pump laser increases, the interference spectrums were recorded and showed in the Fig. 3. When the pump light intensity increased from 0 mW to 15.03 mW, the interference spectrums shifted to the direction of the longer wavelength as shown in the moving direction of the marked by the five-pointed asterisk in Fig. 3. The reason for this result is that as the pump light intensity increases, the resonance of the AuNPs enhances and the heat generated increases. As a result, the optical path difference of the MZI increases and the amount of interference spectrum shift increases.

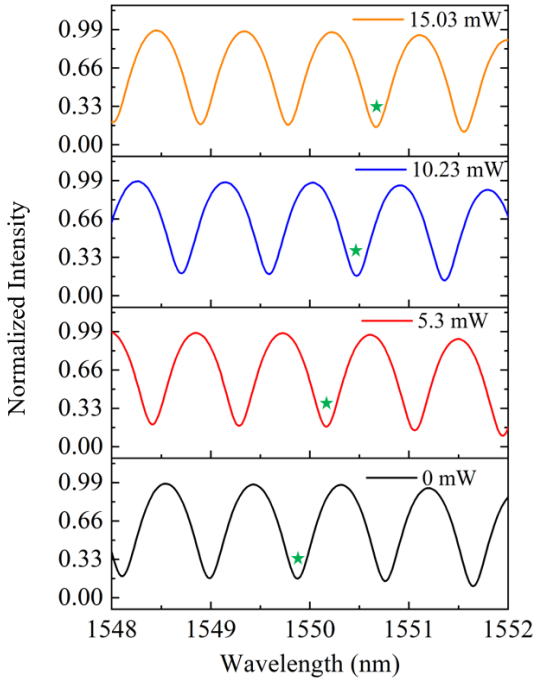

Fig. 3 The interference spectrum shifts with the increase of the pump light intensity.

In order to study the relationship between the intensities of the pump light and the amount of phase shifts, the powers of the pump light were varied from 0 to 50.23 mw at intervals, and the interference spectrum shifted from 1548.98 nm to 1551.66 nm. The results were obtained and shown in the inset of Fig. 4. In this experiment, the maximum spectrum shift is ~2.68 nm, corresponding ~6π (~3 FSRs) phase shifts. From the fitting result, as shown in Fig. 4, we can find that the linear relationship between the pump powers and the phase shifts. What's more, the conversion efficiency of ~0.1 π/mW could be calculated from the slop of Fig. 4. This result should be attributed to the uniform coating of AuNPs on the surface of the microfiber with the assistance of the agarose membrane. Meanwhile, due to the good photothermal ability of the AuNPs embedded in the agarose membrane, the high conversion efficiency can be achieved.

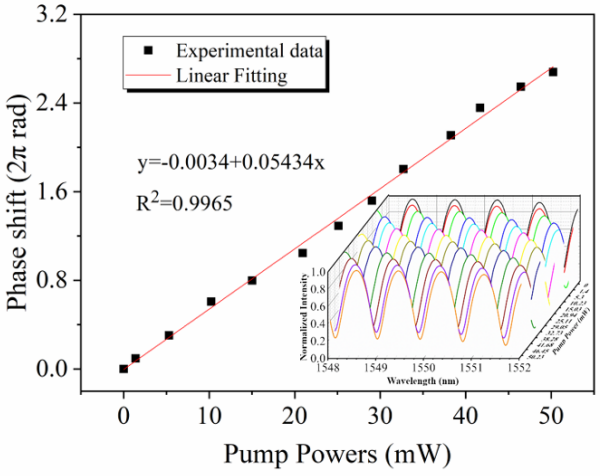

Fig. 4 Linear fitting phase shift and pump light power, the inset shows the phase shifts under different power of pump light.

In subsequent experiments, a single wavelength 1550 nm laser replaced the ASE light source as the signal light, and a monochromator was used to filter out the residual pump light mixed in the signal light at the output end. To explore the all-optical fiber switching capability of the device, the intensity of the single wavelength of 1550 nm was recorded in different powers of pump laser. The results are shown in Fig. 5(a). The position of the wavelength in the interference pattern is shown in the dotted line of the inset. When the powers of pump light increase, the intensities of the single wavelength @ 1550 nm decrease. The transmission extinction ratio was defined as $E_x=[(I_0-I_P)/I_0]\times100\%$. I_0 and I_P are the intensity of the pump laser of 0 and p, respectively. The maximum transmission extinction ration obtained in the experiment is 46.6%. As the power of the pump light increases, the phase shift of the interference spectrum increases. In a half cycle of the interference spectrum, as the phase shift increases, the extinction ratio increases is shown in Fig. 5(b). Theoretically, in this half cycle of the interference spectrum, the maximum transmission extinction ratios can reach to 100% by obtaining a larger interferometric contrast with an optimized structure, for example, adjusting the polarization state of the interference optical path.

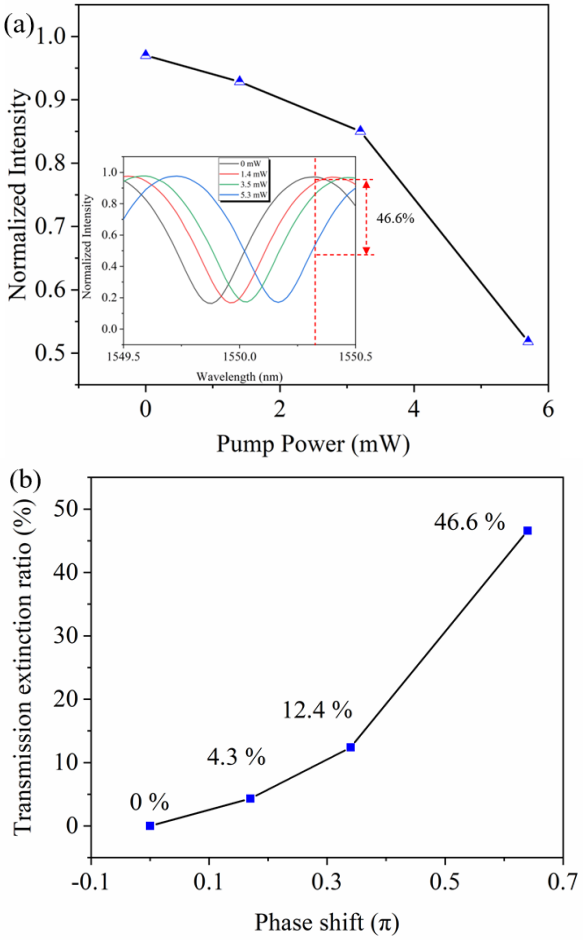

Fig. 5 (a)The output light intensity changes with the pump light intensity. The inset shows the position of the 1550 signals in the interference patterns. (b) In a half of a cycle of the interference, the extinction ratio changes with the amount of phase shift

To further investigate the all-optical switch response capability, an optical chopper (SR540) was placed on the 808

nm coupling optical path to form a pulsed pump light. Real-time monitored and recorded of the single wavelength 1550 nm signal light intensity changing with the 7 Hz pulsed pump light by an oscilloscope. The setup is shown in Fig .6, and the result is shown in Fig. 7. The light intensity presented a periodic change under the pulsed pump light. This result shows that the experimental device has good recovery and reversibility. This may be attributed to the good photo-thermal ability of AuNPs and the good thermal conductivity of the structure.

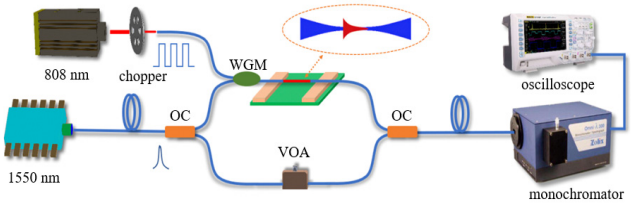

Fig. 6 The schematic diagram of all-fiber switch.

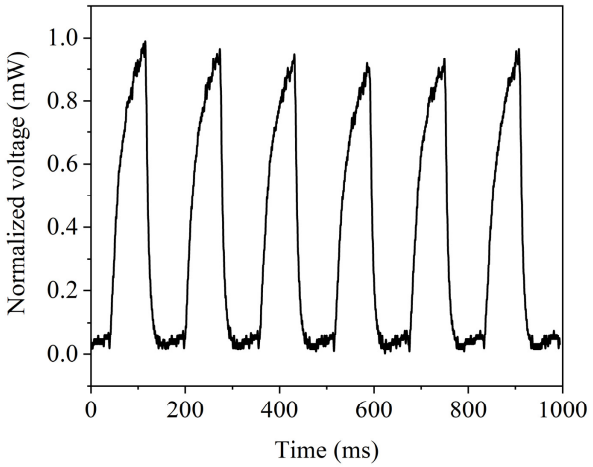

Fig. 7 The waveform of the output signal light with the pulsed pump light.

The dynamic characteristics responses are presented in Fig. 8. By calculating the time of the signal light intensity varies from 10% to 90%, the rising edge time and falling edge time of the device to the pulsed pump light are 47 ms and 14 ms as shown in Fig. 8(a) and Fig. 8(b), respectively. The response times are similar after a series of the same experiments. The rising edge time of the device mainly relied on the LSPR absorption efficiency of the AuNPs and the falling edge time of the device was decided by the heat conduction efficiency between the all-optical switch and the surrounding environment. When the 808 nm light was applied, under the light-to-heat conversion ability of AuNPs, the temperature near the region of the microfiber can reach equilibrium, quickly. When the 808 nm excitation light was turned off, owing to the metal particles well thermal conductivity, the heat exchange time was short between the device and the external environment. Meanwhile, different power pump lights with the same frequency were applied in the all-optical switcher, and the results were shown in the Fig. 9. As the power of the pump light increases, the peak-to-peak voltage (Vpp) and the response time of the signal light within a phase shift period increase significantly. This result should be attributed to the greater phase shift caused by the greater pump power and more heat caused by the instantaneous power. When the frequency of pump light was increased to 10 Hz and 15 Hz, the signal light intensity was recorded. The results are shown in Fig. 10. As the frequency increases, the Vpp decreases and the signal distortion becomes a triangular wave. To further optimize the modulation frequency of the all-optical switch, it is expected to be improved by reducing the diameter of the microfiber such as Ref. [31]. The heat exchange time can be reduced to achieve a higher frequency all-optical switch.

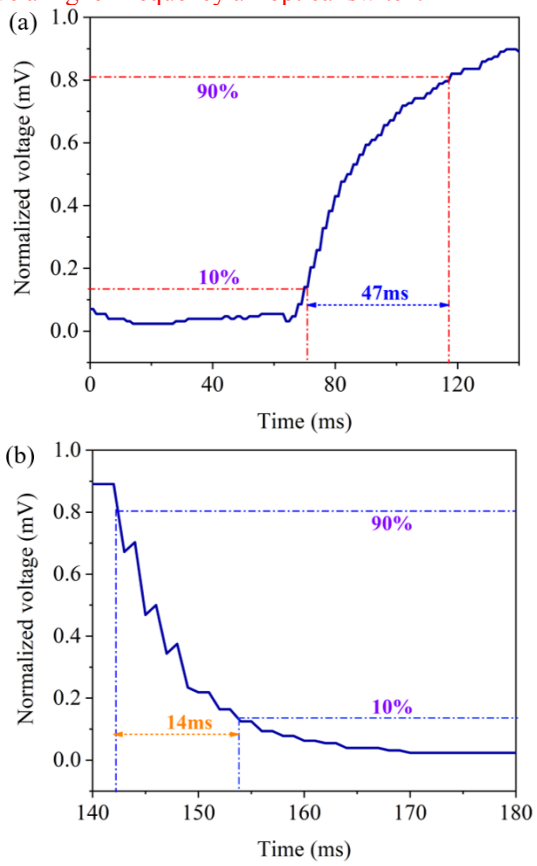

Fig. 8 (a) The rising time and (b) the falling time in one switching cycle.

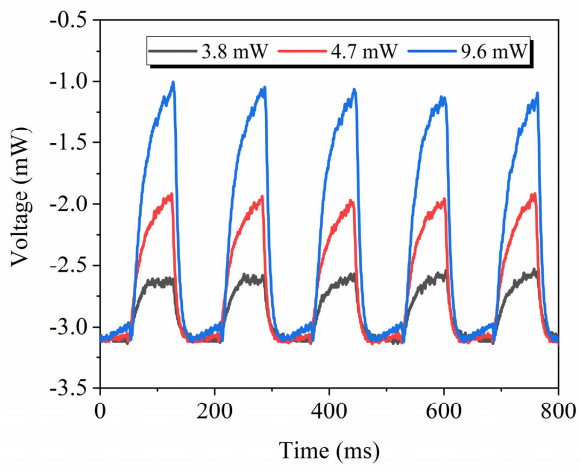

Fig. 9 the output signal intensity of different pump power light.

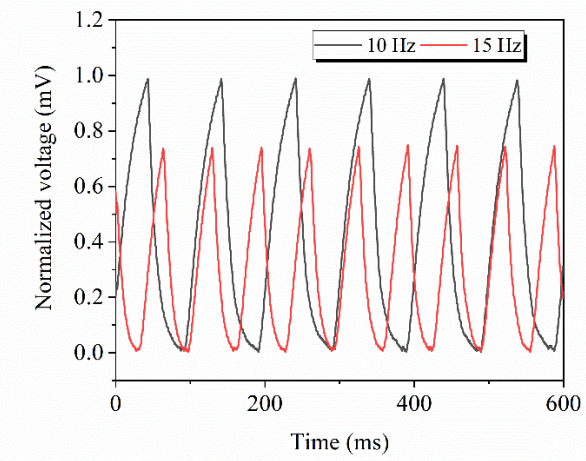

Fig. 10 the output signal intensity of different pump light frequencies

4. Conclusion

In summary, a low loss, low cost, and conveniently prepared all-fiber modulator and switch based on the LSPR absorption of AuNPs is demonstrated. The AuNPs embedded in the agarose membrane were deposited on the surface of the microfiber which was treated with piranha solution. The NIR light excited the AuNPs to generate heat under the LSPR absorption effect and changed the optical path difference of the MZI containing the prepared microfiber. In this work, a series of significant phase shifts were recorded. The maximum phase shift obtained in the experiment is 6π, and the pump power phase shift conversion efficiency is 0.1 π/mW. In addition, an all-optical switch is acquired with rising edge time of 47 ms and falling edge time of 14 ms, and shows great repeatability and reversibility. This low loss, low-cost, and convenient prepared all-fiber phase modulator and switch has great potentials in the all-fiber photonics device.

The authors declare no conflicts of interest.

This work is supported by the National Key R&D Program of China (2018YFC1503703); National Natural Science Foundation of China (NSFC, 11574061, 61405043); the Natural Science Foundation of Heilongjiang Province (LC2018026, F201405); the Fundamental Research Funds for the Central Universities (3072019CF2502); the Key R&D Program of Shaanxi Province (2019GY-073).

1. A. Xomalis, I. Demirtzioglou, E. Plum, Y. Jung, V. Nalla, C. Lacava, K. F. MacDonald, P. Petropoulos, D. J. Richardson and N. I. Zheludev. "Fibre-optic metadevice for all-optical signal modulation based on coherent absorption," Nat. Commun. **9**, 182 (2018).
2. M. Nixon, O. Katz, E. Small, Y. Bromberg, A. A. Friesem, Y. Silberberg and N. Davidson. "Real-time wavefront shaping through scattering media by all-optical feedback," Nat. Photonics. **7**, 919–924 (2013).
3. Y. Zhao, Q. Zhang, X. Xin, Y. Li, R. Gao, Y. Tao, Q. Tian, F. Tian, D. Chen, and G. Cao. "Static resource allocation of advanced reservation requests in elastic optical networks," Appl. Optics. **59**, 1420-1429 (2020).
4. R. Tellez-Limon, S. Blaize, F. Gardillou, V. Coello, and R. Salas-Montiel. "Excitation of surface plasmon polaritons in a gold nanoslab on ion-exchanged waveguide technology," Appl. Optics. **59**, 572-578 (2020).
5. Z. Sun, A. Martinez and F. Wang. "Optical modulators with 2D layered materials," Nat. Photonics. **10**, 227-238 (2016).
6. L. Ye, K. Sui, Y. Zhang and Q. Liu. "Broadband optical wave-guide modulators based on strongly coupled hybrid graphene and metal nanoribbons for near-infrared applications," Nanoscale. **11**, 3229-3239 (2019).
7. P. Li, Y. Wang, and P. Xu. "All-optical logic gates based on unidirectional surface plasmon polaritons," Appl. Optics. **58**, 4205-4210 (2019).
8. Y. Purusothaman, N. R. Alluri, A. Chandrasekhar, V. Venka-teswaran and S. Kim. "Piezophototronic gated optofluidic logic computations empowering intrinsic reconfigurable switches," Nat. Commun. **10**, 4381 (2019).
9. M. Xu, M. He, H. Zhang, J. Jian, Y. Pan, X. Liu, L. Chen, X. Meng, H. Chen, Z. Li, X. Xiao, S. Yu, S. Yu and X. Cai. "High-performance coherent optical modulators based on thin-film lithium niobate platform," Nat. Commun. **11** ,3911 (2020).
10. Y. A. Zaghloul, A. R. M. Zaghloul, and A. Adibi. "Passive all-optical polarization switch, binary logic gates, and digital processor," Opt. Express. **19**, 20332-20346 (2011).
11. W. Yang, W. Gong, C. Hou, Y. Su, Y. Guo, W. Zhang, Y. Li, Q. Zhang and H. Wang. "All-fiber tribo-ferroelectric synergistic electronics with high thermal-moisture stability and comfortability," Nat. Commun. **10**, 5541 (2019).
12. J. Zou, C. Dong, H. Wang, T. Du and Z. Luo. "Towards visible-wavelength passively mode-locked lasers in all-fibre format," Light-Sci. Appl. **9**, 61 (2020).
13. X. Hu, S. Cueff, P. R. Romeo, and R. Orobtchouk. "Modeling the anisotropic electro-optic interaction in hybrid silicon-ferroelectric optical modulator," Opt. Express. **23**, 1699-1714 (2015).
14. M. Li, J. Ling, Y. He, U. A. Javid, S. Xue and Q. Lin. "Lithium niobate photonic-crystal electro-optic modulator," Nat. Commun. **11**, 4123 (2020).
15. Y. Shi, B. Zhang, D. Liu, H. Jiao, X. Wang, N. Liu, and L. Feng. "Linewidth-related residual intensity modulation in lithium niobate phase modulators," Appl. Optics. **59**, 4739-4743 (2020).
16. B. Xu, X. Fan, S. Wang, and Z. He. "Broadband and high-resolution electro-optic dual-comb interferometer with frequency agility," Opt. Express. **27**, 9266-9275 (2019).
17. D. Dung, C. Kurtscheid, T. Damm, J. Schmitt, F. Vewinger, M. Weitz and J. Klaers. "Variable potentials for thermalized light and coupled condensates," Nat. Photonics. **11**, 565–569 (2017).
18. H. Lin, Y. Song, Y. Huang, D. Kita, S. Deckoff-Jones, K. Wang, L. Li, J. Li, H. Zheng, Z. Luo, H. Wang, S. Novak, A. Yadav, C. Huang, R. Shiue, D. Englund, T. Gu, D. Hewak, K. Richardson, J. Kong and J. Hu. "Chalcogenide glass-on-graphene photonics," Nat. Photonics. **11**, 798-805 (2017).
19. E. Lee, S. Choi, H. Jeong, N. Park, W. Yim, M. Kim, J. Park, S. Son, S. Bae, S. Kim, K. Lee, Y. Ahn, K. Ahn, B. Hong, J. Park, F. Rotermund and D. Yeom. "Active control of all-fibre graphene devices with electrical gating," Nat. Commun. **6**, 6851 (2015).
20. X. Ma, H. Sun, Y. Wang, X. Wu and J. Zhang. "Electronic and optical properties of strained noble metals: Implications for applications based on LSPR," Nano Energy. **53**, 932-939 (2018).
21. W. Xu, H. Liu, D. Zhou, X. Chen, N. Ding, H. Song and H. Ågren. "Localized surface plasmon resonances in self-doped copper chalcogenide binary nanocrystals and their emerging applications," Nano Today. **33**, 100892 (2020).
22. L. Xie, X. Yan and Y. Du. "An aptamer based wall-less LSPR array chip for label-free and high throughput detection of biomolecules," Biosens. Bioelectron. **53**, 58-64 (2014).
23. M. Sharifi, F. Attar, A. A. Saboury, K, Akhtari, N. Hoosh-mand, A. Hasan, M. A. El-Sayed and M. Falahatia. "Plasmonic gold nanoparticles: Optical manipulation, imaging, drug delivery and therapy," J. Control. Release. **311-312**, 170-189 (2019).
24. C. Lee, D. E. Oh and T. H. Kim. "Label-free assay of protein kinase A activity and inhibition in cancer cell using electro-chemically-prepared AuNP/rGO nanohybrid electrode modified with C-Kemptide," Talanta. **215**, 120899 (2020).
25. D. Spasopoulos, S. Kaziannis, S. Danakas, A. Ikiades and C. Kosmidis. "LSPR based optical fiber sensors treated with nanosecond laser irradiation for refractive index sensing," Sens. Actuator B-Chem. **256**, 359-366 (2018).

26. R. Chu, C. Guan, Y. Bo, J. Liu, J. Shi, J. Yang, P. Ye, P. Li, J. Yang, and L. Yuan. "Graphene decorated twin-core fiber Michelson interferometer for all-optical phase shifter and switch," Opt. Lett. **45**, 177-180 (2020).
27. M. K. Yazdi, A. Taghizadeh, M. Taghizadeh, F. J. Stadler, M. Farokhi, F. Mottaghitalab, P. Zarrintaj, J. D. Ramsey, F. Seidi, M. R. Saeb and M. Mozafari. "Agarose-based biomaterials for advanced drug delivery," J. Control. Release. **326**, 523-543 (2020).
28. A. Liu, X. Chen, K. Wang, N. Wei, Z. Sun, X. Lin, Y. Chen, and M. Du. "Electrochemical DNA biosensor based on aldehyde-agarose hydrogel modified glassy carbon electrode for detection of PML/RARa fusion gene," Sens. Actuator B-Chem. **160**, 1458-1463 (2011).
29. P. Hashemi, M. Hosseini, K. Zargoosh and K. Alizadeh. "High sensitive optode for selective determination of Ni^{2+} based on the covalently immobilized thionine in agarose membrane," Sens. Actuator B-Chem. **153**, 24-28 (2011).
30. X. Fan, Q. Wang, M. Zhou, F. Liu, H. Shen, Z. Wei, F. Wang, C. Tan, and H. Meng. "Humidity sensor based on a graphene oxide-coated few-mode fiber Mach-Zehnder interferometer," Opt. Express. **28**, 24682-24692 (2020).
31. C. Wang, Y. Z. Wang, X. T. Jiang, Y. F. Song, F. Zhang, J. Liu, and H. Zhang. "Thermal stress-induced all-optical modulation in MXene-coated polarization maintaining fiber," Laser Phys. Lett. **16**, 065107 (2019).